Thermal diffusion, interfacial thermal barrier, and ultrasonic propagation in YBa$_2$Cu$_3$O$_{7-x}$ thin films: Surface-selective transient-grating experiments

C. D. Marshall

Department of Chemistry, Stanford University, Stanford, California 94305

I. M. Fishman

Hansen Experimental Physics Laboratory, Stanford University, Stanford, California 94305

R. C. Dorfman

Department of Chemistry, Stanford University, Stanford, California 94305

C. B. Eom*

Department of Applied Physics, Stanford University, Stanford, California 94305

M. D. Fayer

Department of Chemistry, Stanford University, Stanford, California 94305

The application of interface-selective transient grating experiments to the measurement of anisotropic thermal diffusion constants in thin films of YBa$_2$Cu$_3$O$_{7-x}$ (Y-Ba-Cu-O) is reported. The 50–350-nm-thick Y-Ba-Cu-O films, grown on MgO(100) substrates, are studied using four experimental grating geometries. These provide a measurement of the time-dependent heat flow in the regions adjacent to the Y-Ba-Cu-O/MgO interface, the free film surface, and the bulk of the film. Measurements yield a detailed understanding of the flow of heat from the film into the substrate as well as the direction-dependent diffusion constants. A temperature-dependent thermal barrier that significantly restricts heat transfer from the film into the substrate is observed and quantified. The rate of flow through Y-Ba-Cu-O/MgO interface is ~100 times less than the rate of flow in the Y-Ba-Cu-O film. The anisotropic diffusion constants inside the film have been measured in the 17–300-K temperature range, and the values are found to be similar to those obtained using conventional techniques on bulk samples. The frequency, wave vector, and acoustic damping rate of high-frequency (> 1-GHz) acoustic waves are measured in the same films.

I. INTRODUCTION

In this paper we report a detailed study of heat flow and acoustic-wave propagation in thin films of YBa$_2$Cu$_3$O$_{7-x}$ (Y-Ba-Cu-O) using picosecond transient grating (TG) experiments. TG experiments have been successfully used over the past decade to study the transient responses of a variety of processes, such as diffusion of electronic excited states and phonon excitations or energy transfer between different degrees of freedom of condensed-matter system.[1] The diffracted signal was usually detected in a transmitted diffraction geometry, and the temporal change of dielectric constant induced by two grating excitation beams was studied. In some samples the optical density was so high that the transmitted signal beam could not emerge from the sample, and so the signal was detected with a reflected diffraction geometry.

A more general approach to the transient grating experiments was recently developed.[2] This approach includes the spatial distribution of the grating-induced dielectric-constant profile perpendicular to the grating wave vector. Samples that have spatially distinct physi-

cal properties or have optically generated excitations with nonuniform spatial characteristics will have spatial variations in the grating-induced dielectric constant produced by the excitation beams. For example, surface excitations can have characteristics that are distinct from those in the bulk. The signals obtained from the various geometries can provide information about the time evolution of the grating spatial profile. This approach was qualitatively demonstrated for thin anthracene single crystals[2] and is developed quantitatively in this article for thin high-T_c superconducting Y-Ba-Cu-O films on MgO substrates.

Initial room-temperature results on acoustic-wave excitation and heat flow in Y-Ba-Cu-O thin films using a single transient-grating geometry were published previously.[3] Those results indicated that heating, resulting from two interfering picosecond laser beams, induced surface acoustic (Rayleigh) waves on the sample surface. In addition, it was demonstrated that heat flow through the Y-Ba-Cu-O/MgO interface was limited by a significant thermal barrier. This is clearly indicated by plotting the slowest exponential component of the grating decay, which is proportional to the total amount of heat deposit-

ed in the film, as a function of thickness. Figure 1 displays the longest grating signal decay time for four different sample thicknesses.[3] If there is simple diffusional flow out of the sample into the substrate, the decay time is proportional to the square of the film thickness. If there is a significant barrier to thermal flow out of the film, the decay is linearly proportional to the film thickness. The data in Fig. 1 have a linear thickness dependence demonstrating the existence of a thermal barrier at the interface. Other work utilizing different experimental techniques has indicated that a significant thermal barrier can exist at the Y-Ba-Cu-O–substrate interface.[4,5] All previous experiments were performed over limited temperature ranges, never going below the superconducting transition temperature. Here we report the magnitude of heat flow through the barrier from room temperature to well below the superconducting transition temperature where the barrier is shown to change in magnitude by a factor of 3.

In our initial experiments a single-grating experimental geometry was employed.[3] Since then, theoretical advances[2] show that different geometries can provide a considerably increased amount of information about dynamical processes in a sample. By utilizing various grating excitation and detection geometries, measurements of the thermal profile are made as a function of delay time inside the bulk of the sample, near the film-substrate interface and near the free film surface. Combining the time-dependent measurements from the different geometries leads to a quantitative determination of the anisotropic diffusion constant and the rate of heat flow through the barrier at the Y-Ba-Cu-O/MgO interface. The flow rate through the barrier, which is remarkably slow, is shown to be two orders of magnitude slower than the retardation that is caused by acoustic velocity mismatch at an interface.[6] Several different barrier models will be discussed. Besides the thermal spatial distribution, a detailed description of surface acoustic-wave (Rayleigh-wave) excitation and propagation at high frequencies (> 1 GHz) is given.

II. EXPERIMENTAL PROCEDURES

The output of a Q-switched, mode-locked Nd:YAG laser is frequency doubled to a wavelength of 532 nm and used to drive a sync-pumped dye laser at a wavelength of 561 nm. The dye laser is cavity dumped to produce 45-ps, 20-μJ pulses at a 1-kHz repetition rate. Single dye pulses are attenuated and then split into three beams. Two beams are focused to 300 μm in diameter and crossed at an angle 2θ in a thin ($\sim$ 100 nm) film of highly absorbing Y-Ba-Cu-O on an optically transparent MgO(100) substrate. This produces a sinusoidal interference pattern in the Y-Ba-Cu-O film and generates a grating parallel to the surface, as shown in Fig. 2. Absorption of the light produces electronic excitations which rapidly damp[7] ($\sim$ 1 ps) into the phonon bath, producing a sinusoidal heat pattern in the thin sample. The generation of the thermal grating (or dielectric-constant modulation) leads to a density grating caused by thermal expansion of the Y-Ba-Cu-O film.[8] The rapid deposition of heat with the spatial sinusoidal pattern also generates acoustic waveguide modes with a wavelength equal to the grating wave vector.[9,3] The third pulse, which is the probe, is incident at the Bragg angle from the same side of the sample as the excitation beams.

Both heat and acoustic waves modify the films density in a spatially periodic manner. The density modulations result in changes in the samples complex index of refraction.[8] Modulation of the Y-Ba-Cu-O film's imaginary part of the index of refraction is much greater than the modulation of the real part of the index of refraction. Heat flowing into the substrate can also, in principle, produce a weak signal by modulating the real part of the transparent substrates index of refraction. In MgO thermal diffusion is so fast that there is essentially no periodic density variation. Thus the diffracted signal is dominated by the modulation of the film's optical absorption. Consequently, there is virtually no signal from the thermal modulation of the substrate and the signal arises solely from the thermal distribution inside the film. The probe is temporally delayed and diffracted from the transient holographic grating in both transmission and reflection geometries. The diffracted signal is detected
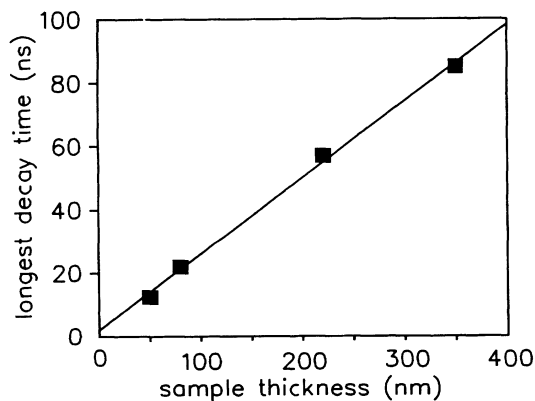

FIG. 1. Inverse of the longest single-exponential time component for a transient-grating signal vs sample thickness. The good agreement between the linear-regression fit of the data points suggests there is a barrier to thermal diffusion at the YBa$_2$Cu$_3$O$_{7-x}$/MgO interface.
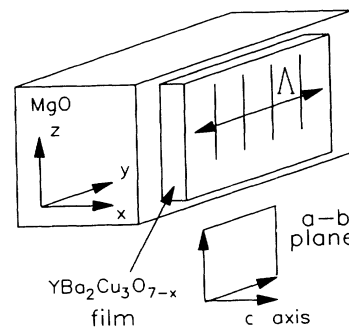

FIG. 2. Transient-grating excitation geometry for thin films on a substrate with the x axis defining the surface normal. The c axis of the film is parallel to the x axis, the a-b plane of the film is parallel to the y-z plane, and the grating wave vector Λ is parallel to the y axis.

with a cooled photomultiplier tube and gated integrator. To improve the signal-to-noise ratio, a computer is used to signal average multiple scans of the delayline.

Experiments are performed in a high-vacuum chamber on c-axis-oriented thin films of Y-Ba-Cu-O (50–350 nm thick) grown on MgO(100) substrates using a 90° off-axis sputtering technique. A detailed description of the sample characteristics and preparation techniques are provided in the literature.[10,11] The electrical resistivity is measured during all experiments using a four-lead method, and the superconducting transition temperature ($R = 0$) is found to be 86 K for all samples used in this study. The grating wave vector is parallel to the film surface, which defines the a-b plane of the sample as shown in Fig. 2. To further improve the signal-to-noise ratio, the excitation and probe beams are orthogonally polarized and the signal detection is polarized parallel to the incident probe polarization. This filters out scattered light from the excitation beams and improved the signal to noise by about one order of magnitude. Separate experiments are performed with the grating excitation beams incident on either the Y-Ba-Cu-O/MgO interface or the Y-Ba-Cu-O/vacuum surface. The grating fringe spacings range from 0.583 to 10.6 μm, and temperatures range from 17 to 300 K. A closed-cycle He refrigerator system with a feedback temperature controller is used to vary the temperature of the sample. The cryostat has a high-vacuum ($\sim 10^{-6}$ Torr) sample chamber (~ 100 mm cube) with 75-mm-diam Pyrex windows to facilitate optical access from a variety of angles. No significant condensation on the sample is detected at a temperature of 15 K over the course of a day. At pressures greater than 10^{-3} Torr, significant condensation takes place, making the optical experiments impossible because of increased scattered light from the sample surface. In addition, condensation is undesirable because it makes the nature of the Y-Ba-Cu-O/vacuum surface uncertain. For each sample excitation geometry, both the reflection and transmission geometries of diffraction are detected.

III. THEORY

A. Diffraction

Consider a film of absorbing material of thickness T on a transparent substrate with the film dielectric constant periodically modulated in the y direction (grating wave-vector direction) as shown in Fig. 2. The grating excitation beams are incident on either the vacuum or substrate side of the film. If the beams are incident on the substrate side, then the axis system which is used is shown in Fig. 2 with the origin at the film-substrate (Y-Ba-Cu-O/MgO) interface. Alternatively, if the beams are incident on the vacuum side, the axis system is rotated about the y axis 180° and the origin is translated to the film-vacuum surface. This permits a derivation of the transient-grating diffraction efficiency with the excitation and probe beams always incident from the negative direction on the $x = 0$ side of the sample. For samples with a large optical density, such as those discussed below, one can neglect the effect of specular reflection from the opposite, or $x = T$, interface of the sample. Treating reflection from only one interface is equivalent to considering a half (semi-infinite) space of modulated material. A general expression for the reflected diffraction efficiency of the probe light intensity has been derived previously,[2]

$$\eta^R(t) = \frac{\omega^2}{c^2} \frac{\cos^2\theta}{|\cos\theta + (\epsilon - \sin^2\theta)^{1/2}|^4} \left| \int_0^T \exp\left[2i\frac{\omega}{c}(\epsilon - \sin^2\theta)^{1/2}x\right] \Delta\epsilon(x,t)dx \right|^2 , \tag{1}$$

and the diffraction efficiency for the transmitted wave is

$$\eta^T(t) = \frac{\omega^2 \cos^2\theta \, e^{-\Omega T}}{4c^2|(\epsilon - \sin^2\theta)^{1/2}[\cos\theta + (\epsilon - \sin^2\theta)^{1/2}]|^2}$$

$$\times \left| \left[\frac{\cos\theta - (\epsilon - \sin^2\theta)^{1/2}}{\cos\theta + (\epsilon - \sin^2\theta)^{1/2}}\right] \int_0^T \exp\left[2i\frac{\omega}{c}(\epsilon - \sin^2\theta)^{1/2}x\right] \Delta\epsilon(x,t)dx + \int_0^T \Delta\epsilon(x,t)dx \right|^2 . \tag{2}$$

The unperturbed dielectric constant of the sample, speed of light, laser frequency, and grating peak-to-null modulation of the dielectric constant are denoted ϵ, c, ω, and $\Delta\epsilon(x,t)$, respectively. The Beer's-law attenuation constant of the probe beam is defined as $\Omega = D\ln(10)/T\cos\theta$, where D is the optical density. A nonabsorbing sample, or a sample with an optical attenuation length much greater than the wavelength of light ($1/\Omega \gg \lambda$), has a reflected diffraction signal [Eq. (1)] which arises strictly from an interface or surface. For highly absorbing samples ($\lambda \simeq 1/\Omega$), the signal is generated in a region within half an absorption length $(2\Omega)^{-1}$ from the surface or interface. The highly absorbing case is the experimental situation, which is discussed in detail below. The first integral in the brackets of Eq. (2) is the surface or interface contribution, and it is equivalent to the integral in Eq. (1). The second integral in Eq. (2) is the bulk contribution and will normally dominate for samples much thicker than the wavelength of light ($T \gg \lambda$). However, for very thin samples ($T \simeq \lambda$), there will be significant contributions from both terms. For the particular experimental case in this paper, the surface term accounts for $\sim 10\%$ of the transmitted signal amplitude.

The preceding expressions are correct for the case of a complex dielectric constant in an absorbing media. The

dielectric constant ϵ and index of refraction n can be explicitly replaced with the substitution

$$\tilde{\epsilon} = \epsilon' + \epsilon'' \tag{3}$$

and

$$\tilde{n} = n_0' + n_0'' \ . \tag{4}$$

All wave vectors are also replaced with the appropriate complex wave vectors. Since the angles used for studying the thermal flow in the x direction are quite small ($\theta = 1.5°$), $|\epsilon| \gg \sin^2\theta$, and Eqs. (1) and (2) can be reduced to

$$\eta^R(t) = \frac{k_0^2}{|1+\tilde{n}_0|^4} \left| \int_0^T e^{2ik_0\tilde{n}_0 x} \Delta\epsilon(x,t) dx \right|^2 \tag{5}$$

and

$$\eta^T(t) = \frac{k_0^2 e^{-\Omega t}}{4|\tilde{n}_0|^2} \left| \int_0^T \left[\frac{1-\tilde{n}_0}{1+\tilde{n}_0} e^{2ik_0\tilde{n}_0 x} + 1 \right] \Delta\epsilon(x,t) dx \right|^2 , \tag{6}$$

where k_0, equal to $2\pi/\lambda$ is the probe wave vector in vacuum. Starting with the complex index of refraction $\tilde{n}_0$ and weakly modulating it with the grating periodicity gives

$$\tilde{n}(x,y,t) = \tilde{n}_0 + \Delta\tilde{n}(x,y,t)$$

$$= (n_0' + in_0'') + \cos(\Lambda y)[\Delta n'(x,t) + i\,\Delta n''(x,t)] , \tag{7}$$

where Λ, the magnitude of the grating wave vector, is equal to $\lambda\pi/2\sin\theta$. Ignoring second-order terms in Δ leads to a modulation of the dielectric constant with a grating peak-to-null amplitude of

$$\Delta\tilde{\epsilon}(x,t) = 2\tilde{n}_0[\Delta n'(x,t) + i\,\Delta n''(x,t)] \ . \tag{8}$$

Since the optically generated electronic excited states have very short lifetimes[7] on the experimental time scale of 0.05–25 ns, only strain-induced contributions to $\Delta n'$ and $\Delta n''$ need be considered. Thus

$$\Delta n'(x,t) = -\Delta S(x,t)\frac{(n_0'^2-1)}{2n_0'} \tag{9}$$

and

$$\Delta n''(x,t) = -\Delta S(x,t)n_0'' \ . \tag{10}$$

Here $\Delta n'$ and $\Delta n''$ are the grating peak-to-null variations in the real and imaginary components of the complex index of refraction due to the presence of strain, respectively. The strain is a result of thermal expansion caused by the heat deposition associated with the rapid radiationless relaxation of the initial electronic excitations. The above contributions to $\Delta n'$ and $\Delta n''$ have been discussed in detail previously.[8] The strain ΔS can be related to the grating peak-to-null termperature difference ΔT by the relation

$$\Delta S(x,t) = \gamma\,\Delta T(x,t) , \tag{11}$$

where γ is the effective thermal-expansion coefficient. To calculate the absolute magnitude of γ, the full anisotropic tensor form of the thermal-expansion coefficient is employed. Calculating γ using the three-dimensional tensor does not change the time dependence of the signal, but could lead to a time-independent signal amplitude dependent on the direction of probe light propagation. Substituting Eqs. (8)–(11) into Eq. (5) yields

$$\eta^R(t) = \frac{K_0^2\gamma^2(C^2+D^2)}{|1+\tilde{n}_0|^4} \left(\left| \int_0^T \cos(2k_0n_0x)e^{-\Omega x}\Delta T(x,t)dx \right|^2 + \left| \int_0^T \sin(2k_0n_0x)e^{-\Omega x}\Delta T(x,t)dx \right|^2 \right) , \tag{12}$$

where

$$C = -2\left[\frac{(n_0'^2-1)}{2} - n_0''^2 \right]$$

and

$$D = -2\left[\frac{(n_0''^2-1)}{2n_0'} - n_0''n_0' \right] ,$$

for the reflected geometry of diffraction. The transmitted diffraction efficiency is obtained by substituting Eqs. (8)–(11) into Eq. (6), which gives

$$\eta^T(t) = M\left| \int_0^T \{ [A_R'\cos(2k_0n_0x) - A_R''\sin(2k_0n_0x)]e^{-\Omega x} + 1 \}\Delta T(x,t)dx \right|^2$$

$$+ M\left| \int_0^T [A_R'\sin(2k_0n_0x) - A_R''\cos(2k_0n_0x)]e^{-\Omega x}\Delta T(x,t)dx \right|^2 , \tag{13}$$

where

$$M = \frac{k_0^2 e^{-\Omega T}(C^2+D^2)\gamma^2}{16|\tilde{n}_0|^2} ,$$

with C and D defined in Eq. (12) A_R' and A_R'' are the real and imaginary components of the electric-field reflection coefficient given by

$$A_R' = \frac{1-n_0'^2-n_0''^2}{(1+n_0')^2+n_0''^2} \tag{14}$$

and

$$A_R'' = \frac{-2n_0''}{(1+n_0')^2+n_0''^2} \ . \tag{15}$$

B. Thermal diffusion

To calculate the time-dependent transient-grating diffraction efficiency, the thermal diffusion equation must be solved with appropriate boundary and initial conditions and the signal must be obtained for the different grating excitation and probe geometries. Only diffusional flow will be considered; i.e., the mean free path of the

phonons is short compared with the sample thickness. The three-dimensional thermal diffusion equation

$$\mathbf{D}\nabla^2 T = \frac{\partial T}{\partial t} \qquad (16)$$

with the initial condition

$$\mathbf{T}(x,y,z,t=0)$$
$$= \frac{T_0}{2} e^{-\Omega x} \left[1 + \cos\left[\frac{2\pi y}{S} \right] \right] e^{-(y^2+z^2)/2a^2} , \qquad (17)$$

is used throughout the paper where S is the grating fringe spacing, T_0 is the initial temperature jump at the incident interface, $\mathbf{D}$ is the anisotropic thermal diffusion constant, and a is the excitation beam radius. The three-dimensional problem can be simplified by separation of variables with the appropriate boundary conditions. The solution takes the form

$$\mathbf{T}(x,y,z,t) = T_0 T(x,t) T(y,t) T(z,t) . \qquad (18)$$

The z-direction thermal profile can be treated as a constant since thermal propagation across the excitation spot size and along a grating fringe crest is negligible on the experimental time scale of 40 ns, i.e., $|\mathbf{D}t/a^2| \ll 1$ for all reasonable $\mathbf{D}$. So, for the purposes of this work,

$$T(z,t) = 1 . \qquad (19)$$

An identical argument holds for diffusion in the y direction across the entire excitation spot size, and the Gaussian laser spot can again be treated as infinite in extent. In the y direction (grating direction), the dielectric constant is sinusoidally modulated by the grating heat profile. This leads to a solution of the form[12]

$$T(y,t) = -\tfrac{1}{2} [1 + e^{-D_y \Lambda^2 t} \cos(\Lambda y)] , \qquad (20)$$

where D_y is the diffusion constant in the y direction.

Diffusion in the x direction (thin direction of the film) is significantly more complicated. Because of the presence of a thermal barrier, an analytic solution is not tractable, but one can obtain numerical solutions. The MgO substrate has a thermal conductivity[13] that is $\sim 10^2$ larger than the thermal conductivity in the c direction of the Y-Ba-Cu-O film.[14] Therefore the MgO substrate will be assumed to be a semi-infinite half-space heat sink such that the temperature profile in the MgO is a constant equal to the equilibrium temperature of the sample. Two different models are used for the barrier-limited diffusivity through the Y-Ba-Cu-O/MgO interfacial region. The first model is a surface conductivity (radiation) boundary condition where the thermal flow across the Y-Ba-Cu-O/MgO interface is proportional to the temperature difference between the two materials. This would be equivalent to an infinitely thin thermal barrier at the Y-Ba-Cu-O/MgO interface, represented mathematically by

$$D\frac{dT}{dx} = A \, \Delta T \bigg|_{\text{Y-Ba-Cu-O/MgO interface}} , \qquad (21)$$

where the temperature drop across the Y-Ba-Cu-O/MgO

interface at $x=0$ is denoted ΔT. The second model is an interfacial layer of a variable thickness ($\sim 1-10\%$ of the total sample thickness) inside the Y-Ba-Cu-O film, where the diffusivity is significantly lower ($\sim 10-100$ times) than that of bulk Y-Ba-Cu-O. For the second model the boundary condition used at the Y-Ba-Cu-O/MgO interface ($x=0$) is $T=T_{\text{eq}}$, where T_{eq} is the equilibrium temperature of the unperturbed substrate before any laser excitation. This implies the absence of any thermal resistance. The finite diffusivity of the interfacial layer is utilized to make the thermal barrier. Both the first and second models would lead to a thermal bottleneck at the interface, but the temporal dependence of the thermal flow for the various detection geometries leads to distinctly different thermal profiles inside the Y-Ba-Cu-O film. At the Y-Ba-Cu-O–vacuum interface, a reflecting (radiationless) boundary condition

$$\frac{dT}{dx} = 0 \bigg|_{\text{Y-Ba-Cu-O/vacuum surface}} \qquad (22)$$

is used since the heat loss from the Y-Ba-Cu-O film into the vacuum is negligible. Since there are two inequivalent interfaces in the problem, the method of images,[15] commonly used to solve simple diffusional problems, leads to a solution that is an infinite summation. The summation converges very slowly and does not provide a practical method for solution of the problem. Consequently, the Crank-Nicholson[16] method is used to obtain numerical solutions that are based on finite differencing the differential equations. This method leads to convergent solutions in a straightforward manner for the initial and boundary conditions used here.

The thermal diffusion solutions must be put in a form which is easily related to the transient-grating observable, i.e., the grating peak-to-null difference in temperature, ΔT.[8] The solution can be written as a sum of two parts:

$$T(x,y,z,t) = \Delta T(x,t)\cos(\Lambda y) + T_c(x,t) . \qquad (23)$$

The first is the grating amplitude and the second is a constant thermal offset T_c [see, for example, the first term in the square brackets of Eq. (20)]. This leads to a grating amplitude term of

$$\Delta T(x,t) = \frac{T_0}{2} e^{-D_y \Lambda^2 t} T(x,t) . \qquad (24)$$

To calculate the transient-grating diffraction intensity, Eq. (24) is substituted into Eqs. (12) and (13), for reflection and transmission diffraction geometries, respectively, and then integrated numerically. Keeping only terms which affect the time dependence of the diffracted signal reduces the normalized diffraction efficiency to

$$\eta^R(t) \propto e^{-2D_y \Lambda^2 t} \left| \int_0^T [a(x) + ib(x)] \Delta T(x,t) dx \right|^2 , \qquad (25)$$

where

$$a(x) = \cos(2k_0 n_0 x) e^{-\Omega x}$$

and

$$b(x) = \sin(2k_0 n_0 x)e^{-\Omega x},$$

for the reflection geometry, and

$$\eta^T(t) \propto e^{-2D_y \Lambda^2 t} \left| \int_0^T [c(x) + id(x)] \Delta T(x,t) dx \right|^2,$$

(26)

where

$$c(x) = [A_R' \cos(2k_0 n_0 x) - A_R'' \sin(2k_0 n_0 x)]e^{-\Omega x} + 1$$

and

$$d(x) = [A_R' \sin(2k_0 n_0 x) - A_R'' \cos(2k_0 n_0 x)]e^{-\Omega x},$$

for the transmission geometry.

IV. RESULTS AND DISCUSSION

A. Thermal flow

Transient grating excitation and detection geometries which emphasize various features of the thermal diffusional process can be used to find the numerical values of the parameters of interest, namely, the anisotropic diffusion constants and details of the barrier conductivity. Figure 3 defines four grating diffraction geometries that are used in the experiments to obtain information on the thermal flow in Y-Ba-Cu-O. When the grating excitation beams are incident on the Y-Ba-Cu-O/MgO interface, as is depicted in Fig. 3(a), the deposition of heat is exponentially weighted (Beer's-law absorption) near that interface. If grating is detected in an interface-reflected (IR) geometry as shown in Fig. 3, then
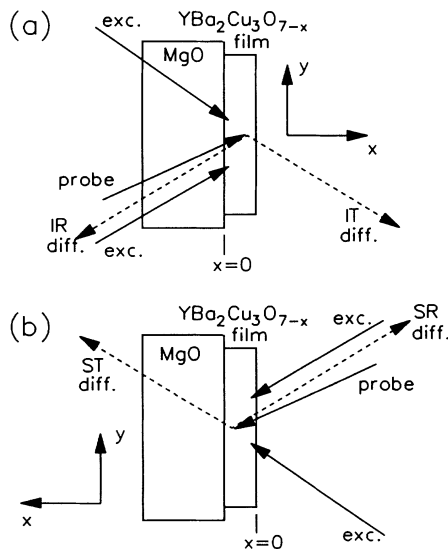

FIG. 3. (a) Interface-reflected (IR) and interface-transmitted (IT) geometries of diffraction where the grating excitation beams are incident on the Y-Ba-Cu-O/MgO interface. (b) Surface-reflected (SR) and surface-transmitted (ST) geometries of diffraction with the grating excitation beams now incident on the Y-Ba-Cu-O/vacuum surface.

the experiment will sample a region very near the Y-Ba-Cu-O/MgO interface since both the generation of the grating and detection of the grating are exponentially weighted near that interface. By detecting the grating in an interface-transmitted (IT) geometry, as shown in Fig. 3, the probe diffracts off each position in the sample with a field amplitude that is proportional to the grating amplitude. This leads to a situation where the signal's spatial origin is only weakly localized near the Y-Ba-Cu-O/MgO interface since the excitation of the grating is initially localized there, but the detection is not.

When the grating excitation beams are incident on the Y-Ba-Cu-O/vacuum surface, as depicted in Fig. 3(b), the deposition of heat is exponentially weighted near the Y-Ba-Cu-O/vacuum surface. If grating is detected in a surface-reflected (SR) geometry, as pictured in Fig. 3, then the experiment will sample a region near the incident surface. The surface-transmitted (ST) detection geometry leads to a less stringent localization of the signal origin. Because of the asymmetric grating excitation, the signal origin is initially weakly localized toward the Y-Ba-Cu-O/vacuum surface, but spreads with time as the heat equilibrates across in the film. In general, the transmitted detection geometry uniformly probes the changes in the dielectric function caused by the temperature profile in the film uniformly throughout the sample. In contrast, the reflected detection geometry samples the change in the dielectric function in a spatially localized region (half of a Beer's absorption length) near the interface or surface on which the probe is incident.

To isolate the effect of diffusion in the plane of the sample (y axis or a-b plane of the Y-Ba-Cu-O film), a transmission geometry of diffraction with a large grating wave vector (small grating fringe spacing) is used. The exponential factor in Eq. (26) depends on the square of the grating wave vector Λ. Thermal flow in the wavevector direction (a-b plane) causes the signal to decay by equalizing the peak-to-null difference in temperature. Flow in the c direction reduces the signal by transferring heat from the film into the substrate. Since thermal diffusion in the a-b plane is substantially faster than in the c direction and the influence of flow in the c direction on the signal is reduced further by the Y-Ba-Cu-O/MgO barrier, the signal decay for large Λ [i.e., $\Lambda \gg (D_{a\text{-}b} t)^{-1/2}$] is dominated by diffusion in the a-b plane. The signal is mildly influenced by the c-axis heat flow, causing a direct single-exponential fit to the data to give a result that is good to within $\sim 10\%$. To obtain more accurate a-b plane thermal diffusion constants, the following method of data analysis is used. The thermal flow into the MgO substrate is independent of the fringe spacing. Hence, at very large fringe spacing where a-b flow is negligible, the time-dependent signal is dominated by the c-direction flow into the substrate [the integral term in Eq. (26)]. Therefore two data sets, one at small (0.583 μm) and one at large fringe spacing (10.6 μm), are divided. This eliminates the time-dependent contribution from the c-direction heat flow and leaves a single-exponential decay, which is solely influenced by a-b plane heat flow.
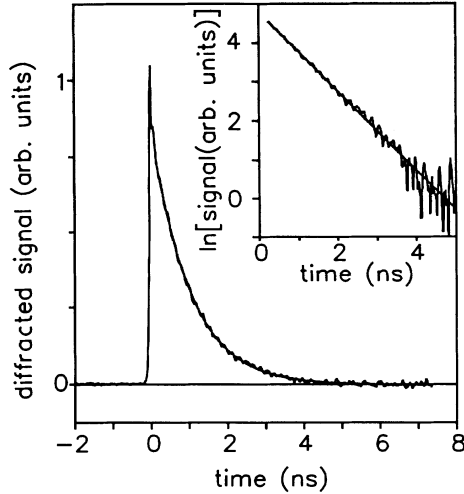
Figure 4 shows divided transient grating data taken at

FIG. 4. Transient-grating signal taken on a 220-nm-thick sample at a fringe spacing of 0.583 μm and a temperature of 80 K in a transmitted diffraction geometry. The data has been corrected to eliminate the effects of diffusion into the substrate. The solid line through the data is a single-exponential fit, and the inset is a logarithmic plot of the same data and fit.

80 K with a single-exponential fit through the data. The inset in Fig. 4 is logarithmic plot of the same data with a linear fit for over four factors of e. Taking Eq. (26) at two fringe spacings and dividing them yields

$$\frac{\eta(t)(\text{small } S)}{\eta(t)(\text{large } S)} = \exp\left[-8D_y\pi t\left[\frac{1}{S_{(s)}} - \frac{1}{S_{(l)}}\right]\right], \quad (27)$$

where $S_{(s)}$ and $S_{(l)}$ are the grating fringe spacings at the small and large spacings, respectively. Using a least-squares algorithm to fit the amplitude and decay of a single exponential to the divided data gives the a-b plane diffusivity directly without reference to or knowledge of the c-axis diffusivity.
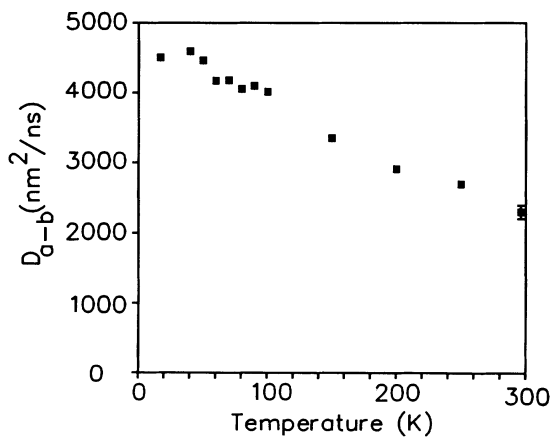

FIG. 5. Temperature dependence of the thermal diffusion constant in the a-b plane of $YBa_2Cu_3O_{7-x}$. The error bar shown on the 300-K data point is representative for all the data points.

Figure 5 displays the a-b plane diffusion constant as a function of temperature from experiments performed on a 220-nm-thick Y-Ba-Cu-O film. The diffusion constant rises smoothly as the temperature is lowered to a value about 2 times larger than that at room temperature. Since the quality of the fits is quite good (see Fig. 4), the error bar shown in Fig. 5 is about ±2% of the maximum parameter value. The largest error in these measurements is due to the uncertainty in measuring the angle between the grating excitation beams, which leads to an uncertainty in the grating wave vector.

The results of Fig. 5 for a-b-plane diffusion are in reasonable agreement with the literature values summarized in Table I that were measured on bulk materials with isotropically mixed a-b-c orientation.[17−22] The reported values for thermal diffusivity vary by a factor of 2, and most are taken on isotropic materials, making comparisons between values for these bulk materials and the oriented thin films incomplete. The variation in the literature values for bulk materials is usually attributed to sample variations arising from different sample preparation methods. Thin-film materials are synthesized using radically different methods than bulk ceramic superconductors. This highlights the need to make accurate measurements on thin-film superconductors. At room temperature the thin-film thermal diffusivity reported here is about 2 times larger than the typical literature value for isotropic bulk samples, but at temperatures near the superconducting transition it falls within the range of literature values shown in Table I. Previous transient-grating experiments gave identical results at room temperature,[3] while work based on the mirage effect,[23] an indirect method, gave diffusivities up to 4 times higher than those reported here.
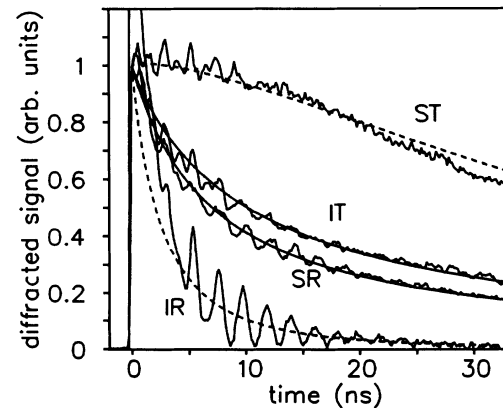

FIG. 6. Transient-grating signals taken at 300 K for the four geometries of diffraction shown in Fig. 3. Curves IR and IT correspond to the interface-reflection and -transmission geometries, respectively, as defined in Fig. 3(a). Curves SR and ST correspond to the surface-reflection and -transmission geometries, respectively, as defined in Fig. 3(b). The two solid curves are theoretical fits to the data with one adjustable parameter each. The dashed curves are theoretical calculations with no adjustable parameters that utilize the material constants determined from the solid-line fits.

MARSHALL, FISHMAN, DORFMAN, EOM, AND FAYER

Using the various grating geometries illustrated in Fig. 3, it is possible to obtain detailed information on the heat flow in the c direction. All of the data used below for determining the c-axis diffusion constant and barrier parameters are taken at a fringe spacing of 10.7 μm in 220-nm-thick samples. At this fringe spacing the data are virtually independent of the a-b plane thermal diffusion since the time required for heat to diffuse a distance comparable to a grating fringe spacing is long compared with the experimental time scale. The a-b plane diffusion does change the large fringe spacing decays by several percent. This contribution is included in the analysis by using the a-b plane diffusion constants (Fig. 5) in the large fringe spacing calculations of the c-axis thermal parameters.

TABLE I. Summary of thermal diffusivity measurements performed on $YBa_2Cu_3O_{7-x}$ taken from the literature and as reported in this work.

Thermal diffusivity (cm^2/s)			
90 K	300 K	Remarks	Reference
0.055		200-μm-thick pellet with mixed a-b-c orientation	17
	0.0017	0.5 mm thick with mixed a-b-c orientation	18
0.014	0.009	1 mm thick with mixed a-b-c orientation	19
0.013	0.007	bulk material mixed a-b-c orientation	20
0.023	0.012	1-mm-thick pellet mixed a-b-c orientation	21
0.005	0.0012	c-axis measurement on oriented $3\times3\times1$-mm^3 single crystal	24
0.0375		160-μm-thick scintered pellet mixed a-b-c orientation	22
	0.046–0.071	thin films with no thickness specified, ZrO_2 substrate conductivity effected result, variations due to annealing differences	23
	0.023	thin films 0.05–0.35 μm thick on MgO a-b plane measurement orientation	3
0.013	0.023	thin films 0.22 μm thick on MgO a-b plane measurement orientation	this work
0.005	0.0028	thin films 0.22 μm thick on MgO c-axis measurement orientation	this work

Figure 6 displays the results of the transient grating experiments taken at temperatures of 296 K in the four geometries described above. The solid and dashed curves through the data, discussed in detail below, are theoretical fits with identical parameters used in all four calculations.

The four geometries give significantly different temporal responses that can be first understood qualitatively. Curve ST in Fig. 6 corresponds to grating excitation from the Y-Ba-Cu-O/vacuum surface and detection in the transmitted geometry of diffraction [Fig. 3(b)]. In a transmitted geometry, the signal is proportional to the total amount of heat deposited or average temperature rise in the sample because of the laser excitation. Since the transmitted signal is generated by heat at any position along the c axis inside the film, the grating signal decays only after the heat is transferred from the absorbing sample film to the transparent MgO substrate. When the excitation beams are incident on the Y-Ba-Cu-O/vacuum surface, the initial heat distribution is localized near the vacuum surface in the film. Before the signal can decay due to heat flow out of the film, it must first diffuse across the entire film thickness to the substrate. In addition, the flow through the Y-Ba-Cu-O/MgO interface is barrier limited. Hence the signal decays slowly over many tens of nanoseconds.

The second transmitted geometry signal is depicted by curve IT in Fig. 6. The grating excitation beams are incident on the Y-Ba-Cu-O/MgO interface in this case [Fig. 3(a)], and the initial thermal distribution inside the film is therefore weighted near the substrate interface. The heat must propagate only a small fraction of the film-thickness before exiting the film. Also, the large initial temperature gradient at the Y-Ba-Cu-O/MgO interface, relative to the previous case where the heat is localized away from the interface, leads to an increased initial flow rate through the barrier. The signal therefore decays several times faster than curve ST in Fig. 6.

Unlike a transmitted diffraction geometry, a reflected geometry can sense the redistribution of heat inside the sample since the signal origin is weighted toward the probe beam's incident interface. In a reflection geometry, the effective probe depth in a highly absorbing material is equal to $\frac{1}{2}$ of a Beer's absorption length as described in Eqs. (25) and (26). For Y-Ba-Cu-O the Beer's absorption length at the experimental wavelength is 66 nm, which leads to an effective exponentially weighted probe depth that is $\sim 10\%$ of the sample thickness.

Curve SR in Fig. 6 corresponds to grating excitation from the Y-Ba-Cu-O/vacuum surface and detection in the reflected diffraction geometry [Fig. 3(b)]. The signal decays rapidly (~ 10 ns) as the heat flows away from the surface and spatially equilibrates. Because the signal arises from a narrow region near the surface, the reflected geometry signal decays several times faster than the transmitted geometry signal with the same grating excitation conditions (curve ST in Fig. 6).

The fastest decaying signal is curve IR in Fig. 6. This corresponds to a reflected diffraction geometry with the grating excitation incident on the Y-Ba-Cu-O/MgO interface. The signal decays due to the heat flow through the barrier into the substrate and to thermal diffusion away from the interfacial region into the bulk of the film. Since this signal is produced near the barrier, it is very sensitive to the details of the barrier model.

To find the numerical value for the c-axis diffusivity, it is necessary to consider a geometry which is insensitive to the specific mechanism of the barrier-limited flow into the MgO. This condition is met by the SR geometry shown in Fig. 3(b). This can be understood by realizing that the thermal excitation is exponentially localized near the vacuum interface. In the reflection geometry, the signal is exponentially weighted near the vacuum interface with a penetration depth of ~ 30 nm. The signal is thus almost solely due to the flow away from the vacuum interface with a negligibly small perturbation due to limited flow through the barrier on the other side of the sample. Using a least-squares fitting procedure, curve SR in Fig. 6 is fitted to the numerical calculations described in Sec. II B with a reflecting boundary condition at both interfaces. A single adjustable parameter fit to the c-axis diffusivity of the Y-Ba-Cu-O thin film is obtained with a magnitude of 290 ± 10 nm^2/ns at 300 K. The procedure resulted in a good quality fit given by the solid line through curve SR in Fig. 6. With the a-, b-, and c-axis diffusivity now defined, specific barrier models can be addressed.

The first model to be considered is the surface conductivity model that corresponds to the boundary condition given in Eq. (21). The IT geometry is the most sensitive to the magnitude of the barrier constant. By varying the value of the barrier constant A [Eq. (21)], it is possible to obtain a high quality least-squares fit for the interface-transmitted geometry. The barrier constant is determined to have a magnitude of 7 ± 1 m/s from the fit to curve IT in Fig. 6. Calculations are performed for the other two geometries (curves ST and IR) using the parameter values defined above (i.e., no adjustable parameters). This serves as a check on the results. The results of these calculations are given by the dashed curves through the IR and ST data sets in Fig. 6. It is apparent that all the calculations are in very good agreement with the data with the exception of the short-time behavior of curve IR in Fig. 6. There is a very fast decay near the initial excitation time with a duration of about 1 ns. The signal for curve IR is primarily generated in the sample region very near (within ~ 10 nm) of the Y-Ba-Cu-O/MgO interface or barrier region. At short time there are several reasons why this signal might not correspond to the simple diffusive behavior utilized to model the data. The interfacial region near the barrier is strained because of lattice mismatch with the MgO. This could lead to different optical, electrical, or mechanical properties such as the optical-absorption constant, heat capacity, or rate of nonequilibrium electron and phonon relaxation. In the absence of a more detailed experimental investigation, it is impossible to tell exactly what the nature of the additional fast-time-scale (<1 ns) dynamics are. The important point is that the long-time-scale dynamics (>1 ns), where the phonons are in equilibrium and more uniformly distributed throughout the film, provide the necessary observable to deduce the thermal flow rate. In addition,

MARSHALL, FISHMAN, DORFMAN, EOM, AND FAYER

calculations are performed with the same barrier model using the literature value of the thermal conductivity in the MgO substrate. This changes the assumption that the substrate acts as an infinite heat sink, to that of a finite sink. The differences in the resulting calculations using the two assumptions are found to be negligible. Therefore the infinite-heat-sink model will be used since the numerical calculations are significantly less complex.

The fitting procedure proved to be very sensitive to the thermal-barrier model. A similar fitting procedure to that described above is performed for the second thermal-barrier model discussed in the theory section. This model, which consists of a surface region of finite thickness (10 Å or more) with a much smaller conductivity than bulk Y-Ba-Cu-O, did not lead to reasonable fits for either curve ST or IR of Fig. 6. Although one can fit some data sets to the second boundary-condition model, it is not possible to find any set of parameters which give reasonable fits to all four possible grating excitation and probe diffraction geometries. This leads to the important conclusion that the physical thickness of the thermal barrier does not exceed the unit-cell size in the c direction of ~ 11 Å. Therefore the model of the "thick barrier" can be eliminated from consideration.

To best visualize the nature of the four different curves given in Fig. 6, it is useful to look at the thermal profiles inside the films. The thermal profiles shown in Fig. 7 are

the results of solving the diffusion equation in the x dimension with the initial and boundary conditions given in Eqs. (17), (21), and (22) and with the parameters obtained from the data in Fig. 6. Parts (a) and (b) of Fig. 7 correspond to the two different excitation geometries defined in parts (a) and (b) of Fig. 3. Each of the five curves in both parts of Fig. 7 correspond to various delay times after the initial excitation which range from 0 to 30 ns. The two curves at zero delay time are spatially exponential, which corresponds to a Beer's-law excitation profile. Each progressive curve becomes flatter in the bulk of the film and slowly drops as a result of heat loss into the MgO substrate. Since the rate of thermal flow into the MgO substrate is slow, the profiles are similar for both excitation directions. This would not be the case if the barrier were eliminated and the temperature at the Y-Ba-Cu-O/MgO interface is equal to the substrate temperature.

Figure 8 gives the c-axis diffusion constant D_c obtained from a series of data sets taken at temperatures from 17 to 300 K using the fitting procedure described above. The diffusion constant is about 10 times smaller than in the diffusion constant in the a-b plane. This is consistent with other thermal-conductivity results obtained on Y-Ba-Cu-O samples.[13] Literature values for the thermal diffusivity in the c direction were obtained from single crystals of Y-Ba-Cu-O.[24] At T_c they are in exact agreement with our results, while at room temperature our results are about 2 times higher. The thermal conductivity is related to the thermal diffusivity through the relation $\textit{k}=\mathcal{D}\rho C_p$, where $\mathcal{D}$, ρ, and C_p are the thermal diffusion constant, density, and heat capacity, respectively. Thermal conductivities reported in the literature are about 10 times larger in the a-b plane than in the c direction.[13] The thermal diffusivity will also be expected to be highly anisotropic since the density and heat capacity are scalars. This implies that our diffusivity results have the same anisotropy as the previous thermal-conductivity measurements on bulk samples.

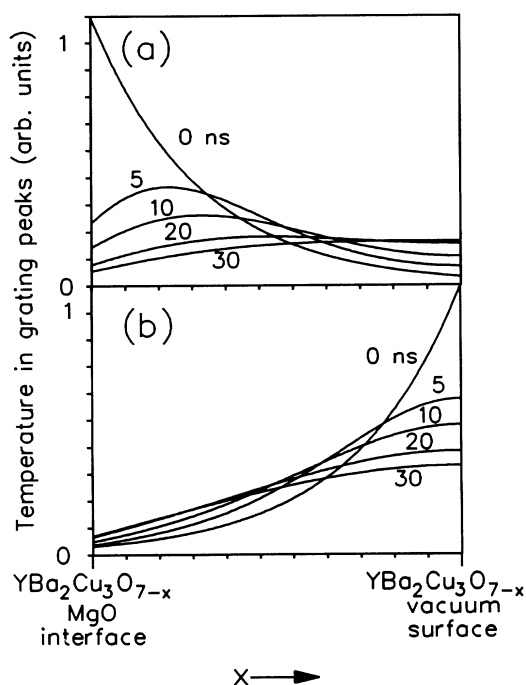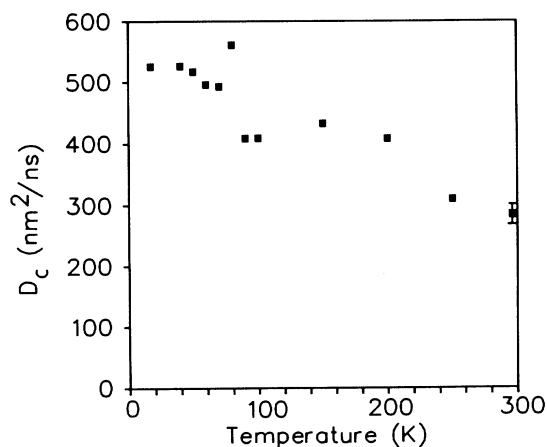The error bar shown in Fig. 8 corresponds to a 2% er-

FIG. 7. Thermal spatial profiles used to calculate the theoretical curves in Fig. 6. Increase in temperature above the equilibrium value in the grating peaks is plotted vs position in the film. Parts (a) and (b) correspond to grating excitation from the Y-Ba-Cu-O/MgO interface and Y-Ba-Cu-O/vacuum surface as shown in Figs. 3(a) and 3(b), respectively. The five curves shown in each part correspond to delays of 0, 5, 10, 20, and 30 ns after the initial thermal excitation.

FIG. 8. Temperature dependence of the thermal diffusion constant in the c-axis direction of $YBa_2Cu_3O_{7-x}$. The error bar shown on the 300-K data point is representative of all the data points.

ror, estimated by fitting several curves at room temperature taken on different days and measuring the spread in the resulting parameters. The diffusion constants rise smoothly as the temperature is lowered. However, there appears to be an anomalous jump at the critical superconducting temperature of 86 K that is about an order of magnitude larger than the estimated experimental error. This jump is noticeably absent in Fig. 5 for the a-b plane diffusivity, making it an interesting feature which may warrant a more detailed investigation. In contrast, other work which discusses anomalous thermal conductivities finds no discontinuities near the superconducting transition temperature in the c direction, while they exist in measurements taken on the a-b plane.[13]

Figure 9 shows the temperature dependence of the barrier constant A, obtained by applying the fitting procedure described above to data sets which ranged in temperature from 17 to 300 K. The error bars in Fig. 9 are much larger than for the diffusion constants because the errors contained in the diffusion constants are propagated into the determination of the barrier constants. Again, the error is estimated by fitting several curves at room temperature and measuring the spread of the numbers which resulted. The dimensions for the barrier constant match those of a velocity, but the barrier constant is $\sim 10^2$ smaller than the velocity of sound in Y-Ba-Cu-O. If one assumes that only phonons (not electrons) participate in heat transfer, then almost all of the phonons have to be reflected from the boundary. The barrier constant A is related to the effective boundary resistance R_{bd} (Ref. 5) through the relation

$$R_{\mathrm{bd}} = \frac{1}{C_p \rho A} , \qquad (28)$$

where C_p and ρ are the heat capacity and density of Y-Ba-Cu-0, respectively. This leads to an effective barrier resistance of 0.5×10^{-3} cm^2 K/W at 300 K. This is in reasonable agreement with previous results in the literature that reported boundary resistances of $\sim 1 \times 10^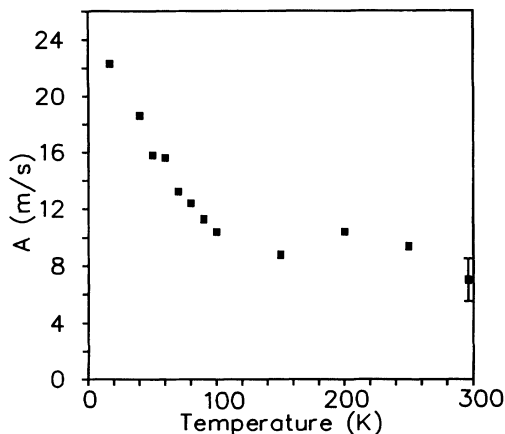{-3}$ cm^2 K/W from 90 to 300 K for Y-Ba-Cu-O films on sapphire substrates[5] and $\sim 1 \times 10^{-3}$ cm^2 K/W at 300 K for Y-Ba-Cu-O films on MgO substrates.[25] The observed value of the barrier constant cannot be explained through acoustic impedance mismatch between the film and substrate.[6,5] A qualitative explanation can be described in terms of poor acoustic contact between the two materials. It is reasonable to expect that Y-Ba-Cu-O will make poor contact with the atomically rough surface of MgO(100). Electron microscopy studies on similar Y-Ba-Cu-O and MgO samples indicate that Y-Ba-Cu-O creates two different crystallographical orientations on the MgO surface.[4] This suggests the idea that poor acoustic contact may be due to voids in the Y-Ba-Cu-O/MgO interfacial region. Poor acoustic contact results in only a small fraction of the interfacial area participating in the process of heat transfer. Since the heat should transfer as the square of the contact area, the results suggest that only 10% of the film area is actually in good contact with the substrate. The hypothesis of poor contact can also explain the observed temperature dependence. The barrier constant rises, corresponding to an increase in thermal flow through the barrier, as the temperature drops below ~ 90 K. Near 90 K there is a discontinuity where the slope changes dramatically. The total change in the barrier constant over the temperature range 17–90 K is about a factor of 3. In comparison, the c-axis thermal diffusivity (Fig. 8) is practically constant over the same range. The temperature dependence of the barrier constant can be explained by considering Rayleigh scattering of the phonons by the interfacial voids. Rayleigh scattering is proportional to the inverse wavelength to the fourth power. As the temperature is lowered, the wavelengths of thermal phonons increase. The mean thermal-phonon wavelength is ~ 10 Å at ~ 90 K where the barrier constant changes slope. The barrier scattering rate would, therefore, decrease abruptly (A increases) as the temperature is lowered past the point where the thermally populated phonons have a wavelength longer than the size of the imperfections at the interface. This implies that the imperfections at the Y-Ba-Cu-O/MgO interface are on the order of 10 Å or approximately the size of a Y-Ba-Cu-O unit cell.

B. Acoustic propagation

Detailed acoustic measurements are also performed on the Y-Ba-Cu-O films. There are pronounced oscillatory components in all of the signals (see Fig. 6), which can be attributed[3] to surface acoustic (Rayleigh) waves.[26] The acoustic portion of the signal is isolated by subtracting off the thermal-flow contribution from the square root of the raw diffraction efficiency data. The results are shown in Fig. 10(a) for data taken on a Y-Ba-Cu-O film 350 nm thick with a grating fringe spacing (acoustic wavelength) of 0.75 μm. To fit the data, it is necessary to include several acoustic modes (different frequencies) (Refs. 26 and 9) and to include a damping for each one. The square root of the acoustic portion of the transient-grating diffraction efficiency, $\sqrt{\eta_{\mathrm{ac}}}$, is fit to a function of the type

FIG. 9. Temperature dependence of the thermal-flow constant A across the YBa$_2$Cu$_3$O$_{7-x}$/MgO interface. The error bar shown on the 300-K data point is representative of all the data points.
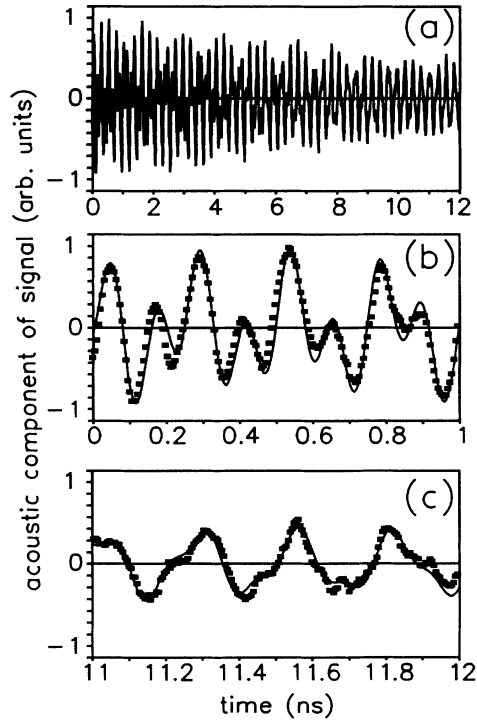
FIG. 10. Acoustic portion of a transient-grating signal at 300 K. The grating fringe spacing is 0.75 μm, and the sample is 350 nm thick. Part (a) shows a fit to the data with two acoustic modes at 3.3 and 8.3 GHz. Parts (b) and (c) are blowups of the first and last 1 ns of part (a).

$$\sqrt{\eta_{ac}} = \sum_i A_i \exp(-\gamma_i t)\cos(\omega_i t + \phi_i) , \qquad (29)$$

where A, γ, ω, and ϕ are the amplitude, damping, angular frequency, and initial phase of each acoustic mode. The data in Fig. 10(a) are fit using Eq. (29) with two acoustic modes at 3.3 and 8.3 GHz. Parts (b) and (c) of Fig. 10 show a blowup of the complete fit for the first and last ns of the data. The high quality of the fit illustrates the accuracy with which the frequency, damping rate, and phase can be obtained.

If the electron-phonon scattering rate were high enough, as is the case with conventional superconductors, the damping rate could provide information on the normal-versus-superconducting electron density.[27] In Y-Ba-Cu-O detailed acoustic damping measurements in the literature show that the electronic component of the damping rate is small.[28–32] This is because of the low ($\sim 10^3$ lower than conventional superconductors) conduction-electron density. This causes a variety of other damping mechanisms, such as defect scattering, to dominate. Figure 11 gives the temperature-dependent damping rate of a 3.7-GHz acoustic wave taken on a 220-nm-thick Y-Ba-Cu-O sample. These results are taken at frequencies about one order of magnitude higher than previous measurements made on Y-Ba-Cu-O. The acoustic propagation direction is parallel to the a-b plane and sample surface. To within the noise, the damping rate (~ 0.05 ns^{-1}) is independent of temperature.
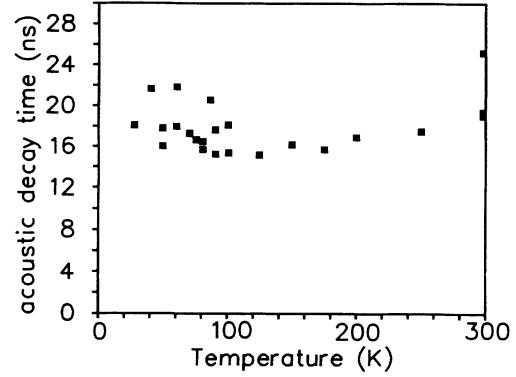

FIG. 11. Temperature dependence of the acoustic damping time for a 3.7-GHz acoustic Rayleigh mode which is propagating in the a-b plane of YBa$_2$Cu$_3$O$_{7-x}$. Data are taken on a 220-nm-thick film with a grating fringe spacing of 0.75 μm.

The initial phase of the acoustic wave at the time of excitation can also be determined from the fit. Like the acoustic damping rate, this is also independent of temperature with a phase shift of less than 5 ps for each acoustic component. This gives an upper limit on the rate of energy transfer from the initial electronic excitation to the very-low-frequency acoustic phonons. Previous work which utilized femtosecond transient optical reflection[7,33] inferred that the electronic relaxation into high-energy phonons occurs in about 1 ps. This study goes one step further and shows that the high-energy phonon subsystem has relaxed within ~ 5 ps to the low-energy acoustic-phonon region, resulting in the thermal expansion and excitation of the acoustic waves that we observe.

V. CONCLUDING REMARKS

This work has demonstrated a nondestructive method capable of measuring the details of the thermal flow in thin films. By utilizing a variety of geometries, this technique can directly determine information on the thermal spatial distribution. Since this method does not require the physical attachment of any transducers or electrical leads, this opens up a regime where thermal flow in all directions can be measured in thin (~ 10 nm or larger) films. The temperature-dependent anisotropic diffusion constants in ~ 100-nm films of YBa$_2$Cu$_3$O$_{7-x}$ have been measured, and the values are found to be similar to those obtained using conventional techniques on bulk samples. A barrier to thermal flow (finite surface thermal conductivity) at the MgO substrate interface has been observed and characterized to have a thickness on the order of the unit-cell size of ~ 11 Å. The barrier thermal-flow rate is found to increase in magnitude by a factor of 3 from room temperature to 17 K.

ACKNOWLEDGMENTS

We would like to thank T. H. Geballe for many informative discussions throughout the course of this research and for providing the high-optical-quality samples used

---

*Present address: AT&T Bell Laboratories, Murray Hill, NJ 07974.

[1]H. J. Eichler, *Laser-Induced Dynamic Gratings* (Springer-Verlag, Berlin, 1986).

[2]I. M. Fishman, C. D. Marshall, J. S. Meth, and M. D. Fayer, J. Opt. Soc. Am. B **8**, 1880 (1991).

[3]C. D. Marshall, I. M. Fishman, and M. D. Fayer, Phys. Rev. B **43**, 2696 (1991).

[4]S. K. Streiffer, B. M. Lairson, C. B. Eom, B. M. Clemens, J. C. Bravman, and T. H. Geballe, Phys. Rev. B **43**, 13 007 (1991).

[5]M. Nahum, S. Verghese, P. L. Richards, and K. Char, Appl. Phys. Lett. **59**(16), 2034 (1991).

[6]W. A. Little, Can. J. Phys. **37**, 334 (1959).

[7]S. D. Borson, A. Kazeroonian, J. S. Moodera, D. W. Face, T. K. Cheng, E. P. Ippen, M. S. Dresselhaus, and G. Dresselhaus, Phys. Rev. Lett. **64**, 2172 (1990).

[8]K. A. Nelson, R. Casalegno, R. J. D. Miller, and M. D. Fayer, J. Chem. Phys. **77**, 1144 (1982).

[9]J. S. Meth, C. D. Marshall, and M. D. Fayer, J. Appl. Phys. **67**, 3362 (1990).

[10]C. B. Eom, J. Z. Sun, S. K. Sun, S. K. Streiffer, A. F. Marshall, K. Yamamoto, B. M. Lairson, S. M. Anlage, J. C. Bravman, T. H. Geballe, S. F. Landerman, and N. R. C. Paber, Physica C **171**, 351 (1990).

[11]C. B. Eom, J. Z. Sun, K. Yamamoto, A. F. Marshall, K. E. Luther, T. H. Geballe, and S. S. Landerman, Appl. Phys. Lett. **55**, 595 (1989).

[12]M. D. Fayer, IEEE J. Quantum Electron. **QE-22**, 1437 (1986).

[13]S. J. Hagen, Z. Z. Wang, and N. P. Ong, Phys. Rev. B **40**, 9389 (1989), and references therein.

[14]Y. S. Touloukian, *Thermophysical Properties of Matter* (Plenum, New York, 1970).

[15]P. R. Wallace, *Mathematical Analysis of Physical Problems* (Dover, New York, 1984).

[16]W. H. Press, B. P. Flannery, S. A. Teokolsky, and W. T. Vetterling, *Numerical Recipes in C* (Cambridge University Press, Cambridge, England, 1988).

[17]M. Marinelli, F. Murtas, M. G. Mecozzi, U. Zammit, R. Pizzoferrato, E. Scudieri, S. Martellucci, and M. Marinelli, Appl. Phys. A **51**, 387 (1990).

[18]J. V. Armstrong, M. McLoughlin, J. G. Luney, and J. M. D. Coey, Superconduct. Sci. Technol. **4**, 89 (1991).

[19]S. B. Peralta, Z. H. Chen, and A. Mandelis, Appl. Phys. A **52**, 289 (1991).

[20]L. Gomez, M. M. F. Vieira, S. L. Baldochi, N. B. Lima, M. A. Novak, N. D. V. Jr., S. P. Morato, A. J. P. Braga, C. L. Cesar, A. F. S. Penna, and J. M. Filho, J. Appl. Phys. **63**, 5044 (1988).

[21]S. B. Peralta, Z. H. Chen, and A. Mandelis, Ferroelectrics **118**, 425 (1991).

[22]F. Murtas, M. G. Mecozzi, M. Marinelli, U. Zammit, R. Pizzoferrato, F. Scudieri, S. Martellucci, and M. Marinelli, in *Photoacoustic and Photothermal Phenomena II*, edited by J. C. Murphy, J. W. Maclachlan-Spicer, L. Aamodt, and B. S. H. Royce (Springer-Verlag, Berlin, 1990).

[23]X. Zhang, C. Gan, Z. Xu, S. Zhang, and H. Zhang, in *Photoacoustic and Photothermal Phenomena II* (Ref. 22).

[24]S. B. Peralta, I. A. Vitkin, K. Ghandi, A. Mandelis, W. Sadowski, and E. Walker, in *Photoacoustic and Photothermal Phenomena II* (Ref. 22).

[25]G. L. Carr, M. Quifada, D. B. Tanner, C. J. Hirschumgl, G. P. Williams, S. Etemad, B. Dutta, F. DeRosa, A. Inam, T. Venkatesan, and X. Xi, Appl. Phys. Lett. **57**, 2725 (1990).

[26]B. A. Auld, *Acoustic Fields and Waves in Solids* (Wiley, New York, 1973), Vol. II, Chap. 10.

[27]W. P. Mason, Phys. Rev. **97**, 557 (1957).

[28]S. Ewert, G. Guo, P. Lemmens, F. Stellmach, J. Wynants, G. Arlt, D. Bonnenberg, H. Kliem, A. Comberg, and H. Passing, Solid State Commun. **64**, 1153 (1987).

[29]P. Lemmens, F. Stellmach, S. Ewert, S. Guo, J. Wynants, G. Arlt, A. Comberg, H. Passing, and G. Marbach, Physica C **153-155**, 294 (1988).

[30]K. J. Sun, W. P. Winfree, M. F. Xu, B, K. Sarma, M. Levy, R. Caton, and R. Selim, Phys. Rev. B **38**, 11 988 (1988).

[31]M. Saint-Paul and J. Y. Henry, Solid State Commun. **72**, 685 (1989).

[32]M. F. Xu, D. Bein, R. F. Wiegert, B. K. Sarma, M. Levy, Z. Zhao, S. Adenwalla, A. Moreau, Q. Robinson, D. L. Johnson, S. J. Hwu, K. R. Poeppelmeier, and J. B. Ketterson, Phys. Rev. B **39**, 843 (1989).

[33]M. E. Gershenson, V. V. Golovlev, I. B. Kedich, V. S. Letokhov, Y. E. Lozovik, Y. A. Matveetz, E. G. Silkis, A. G. Stepanov, V. D. Titov, M. I. Falei, V. M. Farztdinov, S. V. Tchekalin, and A. P. Yartzhev, Pis'ma Zh. Eksp. Teor. Fiz. **52**, 602 (1990).